Pergamon

Int. J. Solids Structures Vol. 33, No. 8, pp. 1137–1156, 1996

0020–7683/96 $15.00 + .00

0020–7683(95)00070–4

A SEGMENTAL APPROACH FOR LARGE THREE-DIMENSIONAL ROD DEFORMATIONS

D. RABOUD, M. G. FAULKNER and A. W. LIPSETT
Department of Mechanical Engineering, University of Alberta, Edmonton, Alberta, Canada T6G 2G8

(*Received* 22 *August* 1994; *in revised form* 8 *March* 1995)

Abstract—The equations of equilibrium for inextensible large three-dimensional deformations of rods are solved using an iterative shooting technique which essentially converts the original boundary value problem to a sequence of initial value problems that converge to the desired solution. This approach is combined with a method for considering the rod using a number of segments. The use of segments in this fashion is found to be useful for modelling complex rod structures, as well as having practical numerical advantages. The technique is applied to a variety of example problems. Where previous analytical or numerical results are available, the present approach is shown to compare favourably. The shooting technique employed is also found to be well suited to finding multiple equilibrium solutions. This method can be used efficiently and accurately on a personal computer, mainly due to the fact that the load can be applied in its entirety so that load increments are not required. In addition, there is no need for large computer memory to store the detailed information for all the segments simultaneously, as the solution of one segment is simply used as the input to the next.

1. INTRODUCTION

While the equations governing the classical Kirchhoff–Clebsch theory for deformations of inextensible elastic rods have been available for some time (Love, 1944), these equations continue to be investigated for several reasons. One of the major reasons for studying solutions is that they have numerous practical applications in problems as diverse as the laying of offshore pipelines (Faulkner and Stredulinsky, 1976–77) and the development of orthodontic retraction systems (Lipsett *et al.*, 1990). A second, very different reason is that the formulation of rod problems is an example of a one-dimensional continuum theory which can be used to investigate nonlinear phenomena including questions of stability (Steigmann and Faulkner, 1993) and multiplicity of solutions (Navaee and Elling, 1992).

When the discussion is limited to planar problems, several analytical results are available for uniform cross-sectional rods subjected to particular loading conditions (Mitchell, 1959; Frisch-Fay, 1962; Antman, 1968–69). For more general loading, especially for the so-called heavy elastica (gravity loading), which require numerical techniques, there is an extensive literature [see the review by Wang (1986)]. The major difficulty in most numerical schemes for large deflection rod problems is the large rotations which can occur between the unloaded and loaded configurations. This can lead to regions where the curvatures become large and, in the case of the finite element and finite difference approaches, require a large number of loading increments, resulting in greatly increased computational effort. Also, in situations for which multiple solutions occur, the usual finite element formulation is not well suited as the loading path must be modified as done by Fried (1981). More recently, Navaee and Elling (1991, 1992) have employed two different approaches to study multiple solutions of cantilever beams. One approach utilizes elliptic integrals and uses a procedure similar to the one developed by Frisch-Fay (1962). The other approach employs a predictor–corrector scheme with an initial value formulation. An alternative approach to either finite element or finite difference formulations, dubbed the segmental technique, was developed for applications including the deployment of offshore pipelines (Faulkner and Stredulinsky, 1976–77) and the prediction of forces and moments produced by specialized orthodontic spring designs (Lipsett *et al.*, 1990; Faulkner *et al.*, 1991). This technique avoids the direct solution of the nonlinear boundary value problem by considering a

sequence of initial value problems similar to that suggested by Keller (1968). With the use of an initial value formulation, the development of multiple solutions can be studied in a systematic manner (Lipsett *et al.*, 1993).

When the truly three-dimensional case is considered, the number of analytical or numerical solutions is more limited. The only tractable analytical solution known to the authors is that of an initially straight circular rod bent and twisted into a helix, which has been considered by Love (1944) for the inextensible case while Whitman and DeSilva (1974) considered the extensible situtation. Numerical solutions for other specific deformations have been given by Frisch-Fay (1962) and more recently by other investigators like Surana and Sorem (1989) using a geometrically nonlinear finite element formulation. With applications for orthodontic springs in mind, Defranco *et al.* (1976) formulated the complete three-dimensional equations; however, they considered only planar examples using a finite difference approach.

A solution procedure utilizing an initial value formulation for fully three-dimensional rod problems is presented in this work. The following section discusses the kinematics, equilibrium equations and constitutive assumptions describing the general behaviour of the rods to be considered. This includes general results which can be used to check the numerical procedure developed later. In Section 3 the nonlinear equations are applied to a segment of the rod and direct numerical integration is used to obtain a solution from the initial values. A method for assembling the various segments together is presented, as well as a shooting technique to ensure boundary conditions are satisfied. Section 4 presents some numerical results for a variety of problems which are compared with previous analytical and numerical results, when available, to assess the effectiveness of the present technique. The first problem considered is an initially straight circular rod bent and twisted into a helix by the action of forces and moments along the initial axis of the rod only. The second problem is an initially straight rod with a rectangular cross-section deformed into a Mobius strip. The third problem considered is an initially curved cantilever beam under the action of dead tip and uniform distributed loads. A final example considers an orthodontic spring which involves an irregular initial configuration.

2. KINEMATICS, CONSTITUTIVE ASSUMPTIONS AND EQUILIBRIUM

For the purpose of this work, a rod is defined to be a one-dimensional continuum which deforms only through bending and twisting, as it is assumed to be inextensible. A reformulation of the theory for such rods in a variational setting has recently been presented in detail by Steigmann and Faulkner (1993). After a brief description of the kinematical basis used, their results will be referred to as required.

A configuration of the rod is characterized by a set of position functions and an orthonormal basis $\{\mathbf{r}(s), \mathbf{e}_i(s)\}$ which define the location and orientation of any point on the rod in terms of the arclength parameter s: $s \in [0, L]$. The vector $\mathbf{e}_1(s)$ is a unit vector which is everywhere in the tangent direction of increasing arc length. The unit vectors $\mathbf{e}_2(s)$ and $\mathbf{e}_3(s)$ are embedded in the material, which defines the orientation of the cross-section. For the case of orthotropic rods, $\mathbf{e}_2(s)$ and $\mathbf{e}_3(s)$ are in the principal directions of the cross-section, while for rods which are transversely isotropic any $\mathbf{e}_2(s)$ and $\mathbf{e}_3(s)$ which span the cross-section are principal directions. This orthonormal basis $\{\mathbf{e}_i(s)\}$ will be referred to as the material basis. In the initially undeformed state $\{\mathbf{r}(s), \mathbf{e}_i(s)\}$ take on the values $\{\mathbf{x}(s), \mathbf{E}_i(s)\}$, which serves as a reference configuration. The material basis $\{\mathbf{e}_i\}$ differs from the Frenet basis in that the latter depends only on the shape of the centreline of the rod and does not take the orientation of the cross-sections into account. The material basis has the advantage of being uniquely determined even in the case where the rod remains straight.

The rate of change of the material basis $\{\mathbf{e}_i\}$ with respect to arc length is determined by the vector $\boldsymbol{\kappa}$ ($\boldsymbol{\kappa} = \kappa_j \mathbf{e}_j$), i.e.

$$\mathbf{e}_i' = \boldsymbol{\kappa} \times \mathbf{e}_i, \tag{1}$$

where the prime notation indicates differentiation with respect to arc length. The κ_1 component is the twist per unit length along the rod, while κ_2 and κ_3 are the components of

curvature. In the rod's undeformed configuration, which may be initially curved and twisted, $\kappa_i(s)$ take on the values $\kappa_i^0(s)$.

The equations of equilibrium can be derived from variational principles (Steigmann and Faulkner, 1993) or from more elementary considerations (Love, 1944; Landau and Lifshitz, 1986) and are

$$\mathbf{F}' + \mathbf{b} = \mathbf{0}$$
$$\mathbf{M}' = \mathbf{F} \times \mathbf{e}_1, \tag{2a,b}$$

where $\mathbf{F}$, $\mathbf{M}$ and $\mathbf{b}$ are the normal force resultant, moment resultant and body force per unit length, respectively.

It has been shown (Steigmann and Faulkner, 1993) that for rods which are uniformly curved and twisted in the reference configuration, the classical energy integral (Love, 1944) can be generalized to give

$$U - \boldsymbol{\kappa} \cdot \mathbf{M} - \mathbf{e}_1 \cdot \mathbf{F} - \mathbf{r} \cdot \mathbf{b} = \text{const}, \tag{3}$$

where U is the strain energy per unit length and $\mathbf{b}$ is a constant body force. This result can serve as an accuracy check, which must be approximately satisfied by any numerical technique.

The rods being considered are assumed to have a quadratic strain energy function U. As is the usual case (Love, 1944), it is further assumed that U depends only on the difference between the initial and final components of curvature, according to

$$U = \tfrac{1}{2}[GJ(\kappa_1 - \kappa_1^0)^2 + EI_2(\kappa_2 - \kappa_2^0)^2 + EI_3(\kappa_3 - \kappa_3^0)^2], \tag{4}$$

where GJ is the torsional rigidity and EI_2 and EI_3 are the flexural rigidities about the principal $\mathbf{e}_2$ and $\mathbf{e}_3$ axes, respectively. This in turn implies that the moment can be expressed as

$$\mathbf{M} = GJ(\kappa_1 - \kappa_1^0)\mathbf{e}_1 + EI_2(\kappa_2 - \kappa_2^0)\mathbf{e}_2 + EI_3(\kappa_3 - \kappa_3^0)\mathbf{e}_3. \tag{5}$$

When the rod being considered is initially straight and transversely isotropic, there is the special result that

$$\kappa_1 = \text{constant} \tag{6}$$

(Landau and Lifshitz, 1986), which must be satisfied. This can also serve as an accuracy check on the results delivered by any numerical technique for problems in this class.

3. NUMERICAL PROCEDURE

Consider a segment of the rod as shown in Fig. 1. As will be discussed later, a number of these segments will be joined together to form the complete rod. Here, $\{\mathbf{E}_i\}$ is a fixed

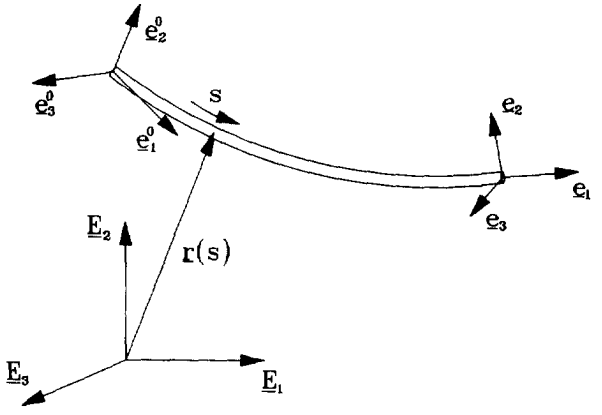

Fig. 1. Arbitrary rod segment.

global orthonormal basis in which the particular rod problem is formulated. For example, if gravity loading is included it may act in the negative, $\mathbf{E}_2$ direction. $\{\mathbf{e}_i\}$ is the embedded material basis which changes orientation along the length of the rod segment. At the start of the segment ($s = 0$) the values of $\{\mathbf{e}_i\}$ are $\{\mathbf{e}_i^0\}$, which will serve as a fixed (independent of arclength) basis in a particular segment of the rod. The basis $\{\mathbf{e}_i^0\}$ will be referred to as the local basis.

The orientation of the material basis in terms of the local basis is most conveniently expressed using Euler angles. Love (1944) used a set of Euler angles which suffer from the fact that a singularity occurs for a null rotation. For convenience, the set of Euler angles commonly referred to as the yaw (ϕ), pitch (θ) and roll (ψ) angles [see Goldstein (1980)] are chosen which move the singularity away from the null rotation. In terms of these angles the components of the material basis $\{\mathbf{e}_i\}$ are

$$\begin{Bmatrix} \mathbf{e}_1 \\ \mathbf{e}_2 \\ \mathbf{e}_3 \end{Bmatrix} = [R] \begin{Bmatrix} \mathbf{e}_1^0 \\ \mathbf{e}_2^0 \\ \mathbf{e}_3^0 \end{Bmatrix}, \tag{7}$$

$$[R] = \begin{bmatrix} c_\theta c_\phi & c_\theta s_\phi & -s_\theta \\ s_\psi s_\theta c_\phi - c_\psi s_\phi & s_\psi s_\theta s_\phi + c_\psi c_\phi & c_\theta s_\psi \\ c_\psi s_\theta c_\phi + s_\psi s_\phi & c_\psi s_\theta s_\phi - s_\psi c_\phi & c_\theta c_\psi \end{bmatrix}, \tag{8}$$

where c and s represent cosine and sine, respectively. Therefore, the Euler angles at the start of the segment are $\{0, 0, 0\}$ (i.e. a null rotation).

The components of curvature and twist along the segment, which are shown (Steigmann and Faulkner, 1993) to be

$$\kappa_i = \tfrac{1}{2} e_{ijk} \mathbf{e}_k \cdot \mathbf{e}_j', \tag{9}$$

where e_{ijk} is the permutation symbol, can then be expressed in terms of the Euler angles as

$$\begin{aligned} \kappa_1 &= \psi' - s_\theta \phi', \\ \kappa_2 &= c_\theta s_\psi \phi' + c_\psi \theta', \\ \kappa_3 &= c_\theta c_\psi \phi' - s_\psi \theta'. \end{aligned} \tag{10}$$

In terms of the local basis, the rod segment starts at the local coordinates $(x, y, z) = (0, 0, 0)$. Since $\mathbf{e}_1 = \mathbf{r}'(s)$ is the unit tangent vector, the coordinates of the centreline of the rod in the local basis satisfy the differential equations

$$x' = c_\theta c_\phi, \quad y' = c_\theta s_\phi, \quad z' = -s_\theta. \tag{11}$$

The force vector $\mathbf{F}$ at the start of the segment can be expressed as

$$\mathbf{F} = F_i^0 \mathbf{e}_i^0, \tag{12}$$

where the F_i^0 are the initial tension and shear components. For the purpose of illustration, consider that a dead uniform distributed load $\mathbf{b}$ acts on the segment. $\mathbf{b}$ can be expressed in terms of $\{\mathbf{e}_i^0\}$, since this is a valid orthonormal basis, as

$$\mathbf{b} = b_i \mathbf{e}_i^0, \tag{13}$$

where the b_i are constants. The equilibrium equation (2a) can then be integrated to give

$$\mathbf{F}(s) = \mathbf{F}(0) - \int_0^s \mathbf{b}\,\mathrm{d}s, \tag{14}$$

which for the special case of uniform loading becomes

$$\mathbf{F}(s) = (F_i^0 - b_i s)\mathbf{e}_i^0. \tag{15}$$

However, to obtain the true tension and shear components along the segment, $\mathbf{F}$ needs to be expressed in terms of the material basis so that

$$\mathbf{F} = F_i \mathbf{e}_i, \tag{16}$$

where

$$\begin{Bmatrix} F_1 \\ F_2 \\ F_3 \end{Bmatrix} = [R] \begin{Bmatrix} F_1^0 - b_1 s \\ F_2^0 - b_2 s \\ F_3^0 - b_3 s \end{Bmatrix}. \tag{17}$$

Combining the constitutive relationship (5) with the equilibrium equation (2b) gives

$$\begin{aligned} \mathbf{F} \times \mathbf{e}_1 = {} & GJ(\kappa_1 - \kappa_1^0)\mathbf{e}_1' + EI_2(\kappa_2 - \kappa_2^0)\mathbf{e}_2' + EI_3(\kappa_3 - \kappa_3^0)\mathbf{e}_3' \\ & + GJ\kappa_1'\mathbf{e}_1 + EI_2\kappa_2'\mathbf{e}_2 + EI_3\kappa_3'\mathbf{e}_3, \end{aligned} \tag{18}$$

which can be written as three component equations:

$$\begin{aligned} GJ\kappa_1' &= (EI_2 - EI_3)\kappa_2\kappa_3 + EI_3\kappa_2\kappa_3^0 - EI_2\kappa_3\kappa_2^0, \\ EI_2\kappa_2' &= (EI_3 - GJ)\kappa_1\kappa_3 + GJ\kappa_3\kappa_1^0 - EI_3\kappa_1\kappa_3^0 + F_3, \\ EI_3\kappa_3' &= (GJ - EI_2)\kappa_1\kappa_2 + EI_2\kappa_1\kappa_2^0 - GJ\kappa_2\kappa_1^0 - F_2. \end{aligned} \tag{19}$$

Note that the tension F_1 is not involved directly since the rod is assumed to be inextensible. By introducing the dimensionless parameters

$$\begin{gathered} \rho = \frac{s}{L}, \quad \hat{\kappa}_i = \kappa_i L, \quad \nu_i = \frac{F_i L^2}{EI}, \quad \chi_i = \frac{b_i L^3}{EI}, \\ \Omega = \frac{GJ}{EI}, \quad \beta = \frac{EI_2}{EI}, \quad \gamma = \frac{EI_3}{EI}, \end{gathered} \tag{20}$$

where EI (no subscript) is taken to be the larger of EI_2 and EI_3, eqns (19) become a dimensionless system of three second order differential equations for the three Euler angles:

$$\begin{aligned} \ddot{\phi} &= \frac{\hat{C}_1\beta c_\psi + \hat{C}_2\gamma s_\psi}{\beta\gamma c_\theta}, \\ \ddot{\theta} &= \frac{\hat{C}_2\gamma c_\psi - \hat{C}_1\beta s_\psi}{\beta\gamma}, \\ \ddot{\psi} &= \frac{\hat{C}_3 + \Omega s_\theta \ddot{\phi}}{\Omega}, \end{aligned} \tag{21}$$

where

$$\hat{C}_1 = (\Omega-\beta)\hat{\kappa}_1\hat{\kappa}_2+\beta\hat{\kappa}_2^0\hat{\kappa}_1-\Omega\hat{\kappa}_1^0\hat{\kappa}_2+\gamma(s_\theta c_\psi\dot{\phi}\dot{\theta}+c_\theta s_\psi\dot{\phi}\dot{\psi}+c_\psi\dot{\theta}\dot{\psi})-v_2,$$

$$\hat{C}_2 = (\gamma-\Omega)\hat{\kappa}_1\hat{\kappa}_3+\Omega\hat{\kappa}_1^0\hat{\kappa}_3-\gamma\hat{\kappa}_3^0\hat{\kappa}_1+\beta(s_\theta s_\psi\dot{\phi}\dot{\theta}-c_\theta c_\psi\dot{\phi}\dot{\psi}+s_\psi\dot{\theta}\dot{\psi})+v_3,$$

$$\hat{C}_3 = (\beta-\gamma)\hat{\kappa}_2\hat{\kappa}_3+\gamma\hat{\kappa}_3^0\hat{\kappa}_2-\beta\hat{\kappa}_2^0\hat{\kappa}_3+\Omega c_\theta\dot{\phi}\dot{\theta}, \tag{22}$$

and where the superposed dot indicates differentiation with respect to ρ. Similarly, using eqn (20), eqns (10) and (17) become

$$\hat{\kappa}_1 = \dot{\psi}-s_\theta\dot{\phi},$$

$$\hat{\kappa}_2 = c_\theta s_\psi\dot{\phi}+c_\psi\dot{\theta},$$

$$\hat{\kappa}_3 = c_\theta c_\psi\dot{\phi}-s_\psi\dot{\theta}, \tag{23}$$

and

$$\begin{Bmatrix} v_1 \\ v_2 \\ v_3 \end{Bmatrix} = [R]\begin{Bmatrix} v_1^0-\chi_1\rho \\ v_2^0-\chi_2\rho \\ v_3^0-\chi_3\rho \end{Bmatrix}, \tag{24}$$

while eqn (11) becomes simply

$$\frac{\dot{x}}{L} = c_\theta c_\phi, \quad \frac{\dot{y}}{L} = c_\theta s_\phi, \quad \frac{\dot{z}}{L} = -s_\theta. \tag{25}$$

Equations (20)–(25) completely describe the deformation of the rod segment in terms of the conditions at the beginning of that segment. The forces, moments and geometry at the end of the segment can therefore be determined by the forces, moments and geometry at the start of the segment by direct numerical integration. The geometry obtained along the rod is then related back to the global basis $\{\mathbf{E}_i\}$ to allow the specific position of the rod to be determined. The Bulirsch–Stoer method is used, rather than the more common Runge–Kutta methods, to perform the integration because it is significantly more computationally efficient when high precision is required [see Press *et al.* (1992) for a description of the method].

In the previous discussion a method of solution for an individual segment of the rod was presented. To solve the entire rod, which can be composed of a number of segments, the individual segments are assembled in such a way that force and geometric compatibility are maintained. This is accomplished by using the values for the forces and geometry obtained at the end of one segment as the starting values to the next. For example, the orientation of the material basis $\{\mathbf{e}_i\}$ at the end of the kth segment becomes the local basis $\{\mathbf{e}_i^0\}$ for the $k+1$th segment. This procedure is continued from segment to segment until a solution is obtained for the entire rod. In this way, the forces, moments and geometry at the end of the rod are completely determined by the forces, moments and geometry at the start of the rod.

One of the main reasons for solving the rod in segments in this manner is that many rods of interest have complicated geometries in their undeformed configuration. These rods can be modelled as a series of segments of simple geometric types. Since each individual segment has a simple geometry it can be considered much more readily. Complex loading conditions or varying material properties can be similarly handled in a straightforward manner. A further advantage to using segments is that for many problems large rotations occur and the Euler angles used can pass through a singular point ($\theta = \pi/2$ for the Euler angles used here). By introducing new segments along the rod, the Euler angles can all be reset to zero, thus avoiding the singularity and the resulting numerical difficulties.

The solution as presented is an initial value approach in that the conditions must be completely specified at one end of the rod in order to obtain a solution. Most rod problems are actually two-point boundary value problems where some of the boundary conditions

are known at each end of the rod. To solve such a problem an iterative shooting procedure, similar to that described in detail for planar problems (Lipsett *et al.* 1990), is employed. This procedure requires that 12 initial conditions (force and moment components, position coordinates and Euler angles to specify the orientation) be specified at the start of the rod. In general, not all of these will be known *a priori*. Some of these values will be unknown, but a corresponding number of conditions will be known at the other end of the rod. The unknowns must be initially estimated to start the numerical procedure. From these initial conditions the solution throughout the rod is obtained using the method described. However, as the computed conditions at the end of the rod will not in general agree with the known conditions at that end, a Newton–Raphson false position method is then used to iteratively improve the estimates of the unknown initial values until the required boundary conditions at the end of the rod are satisfied to within some specified tolerance.

4. RESULTS AND APPLICATIONS

To illustrate the numerical technique described in the previous section, four problems are presented. The first problem which will be considered is that of an initially straight circular rod deformed into a helix with radius R and pitch angle α by the application of moments and forces along the initial axis of the rod only (Fig. 2). The analytical solution, which has been presented by Love (1944) and Landau and Lifshitz (1986), requires a moment of

$$\mathbf{M} = M_z\mathbf{E}_3 + M_\zeta\mathbf{E}_\zeta, \tag{26}$$

where

$$M_z = GJ\kappa_1 \sin\alpha + \frac{EI}{R}\cos^3\alpha,$$

$$M_\zeta = GJ\kappa_1 \cos\alpha - \frac{EI}{R}\cos^2\alpha \sin\alpha,$$

$$\mathbf{E}_\zeta = -\sin\zeta\mathbf{E}_1 + \cos\zeta\mathbf{E}_2, \tag{27a–c}$$

where M_z is the component of the moment along the initial axis of the rod, M_ζ is the component tangential to the cylinder on which the helix is traced, ζ is the angle of rotation about the $\mathbf{E}_3$ axis and $EI_z = EI_3 = EI$. In addition, the force required is

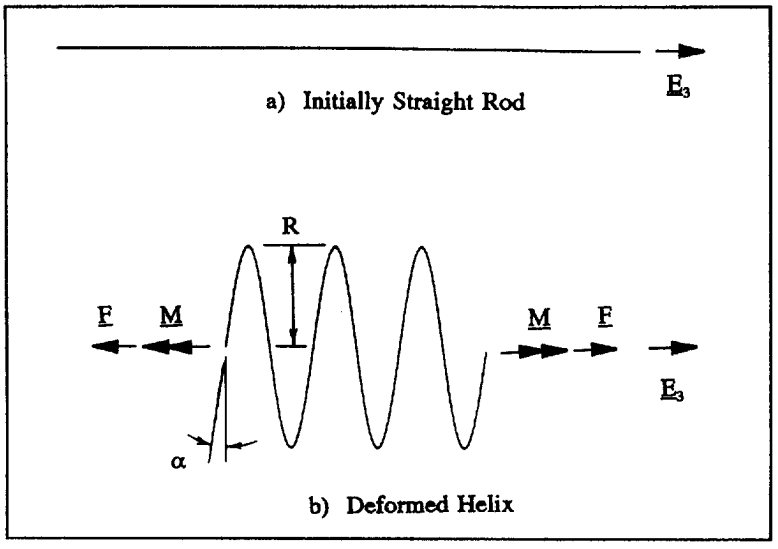

Fig. 2. Straight rod deformed into a helix.

$$\mathbf{F} = F\mathbf{E}_3,$$

$$F = \frac{GJ\kappa_1}{R} - \frac{EI}{R^2}\cos^2\alpha\sin\alpha, \tag{28}$$

so that

$$M_\zeta = FR. \tag{29}$$

If the problem is posed with M_z, F and α specified, the radius R and the twist per unit length κ_1 are determined using eqns (27a, b) and (29) to yield

$$R = \frac{\cos\alpha}{2F\sin\alpha}[M_z \pm \sqrt{M_z^2 - 4EIF\sin\alpha}], \tag{30}$$

with the corresponding value for κ_1 determined from either of eqns (27a, b). This means that there may be either no solution or two solutions for the radius (each with a corresponding κ_1) provided $F \neq 0$.

To begin the solution procedure the coordinates of the start of the rod in the global basis are assumed to be

$$X = R, \quad Y = 0, \quad Z = 0, \tag{31}$$

while the initial material basis is given by

$$\begin{aligned} \mathbf{e}_1 &= \cos\alpha\mathbf{E}_2 + \sin\alpha\mathbf{E}_3, \\ \mathbf{e}_2 &= \mathbf{E}_1, \\ \mathbf{e}_3 &= \sin\alpha\mathbf{E}_2 - \cos\alpha\mathbf{E}_3, \end{aligned} \tag{32}$$

for a helix with pitch angle α. This allows the force and moment components relative to the material basis to be calculated at the start of the rod.

To compare the numerical and analytical solutions, an initially straight steel rod ($E = 207$ GPa, $G = 70$ GPa) of length 1 m and with a cross-sectional diameter of 6 mm is subjected to axial forces and moments of 100 N and 200 Nm respectively, with the pitch angle α selected to be 45°. This particular choice of forces allows two analytical solutions from eqn (30) as

$$\begin{aligned} (R)_1 &= 0.04769610\,\text{m} \quad (\kappa_1)_1 = 16.25726757\,\text{m}^{-1}, \\ (R)_2 &= 1.95230390\,\text{m} \quad (\kappa_1)_2 = 31.37851470\,\text{m}^{-1}. \end{aligned} \tag{33a,b}$$

Figure 3 is a plot of the deformed geometry in the ZY and ZX planes for both the analytical solutions and the numerical results. (Note: the XY plane geometry is a circular arc.) The numerical solutions can be seen to be indistinguishable from the analytical solutions. While the first solution (33a) indicates a helix with more than two complete turns, the second is only a small fraction of one turn. Since the initial conditions are completely specified, no shooting is required to solve this problem. Note that despite the simple initial geometry, five segments were required to generate the numerical solution. This was in order to avoid the singularity in the Euler angles which would occur at an arclength of approximately 0.211 m and cause numerical difficulties.

As well as comparing the deformed shapes as above, two further checks on the accuracy of the numerical solution were done. As this is a circular rod the twist per unit length κ_1 should remain a constant. In addition, the first integral [eqn (3)] should also be a constant. There was no variation in either of these quantities to seven significant digits for the two numerical solutions shown in Fig. 3.

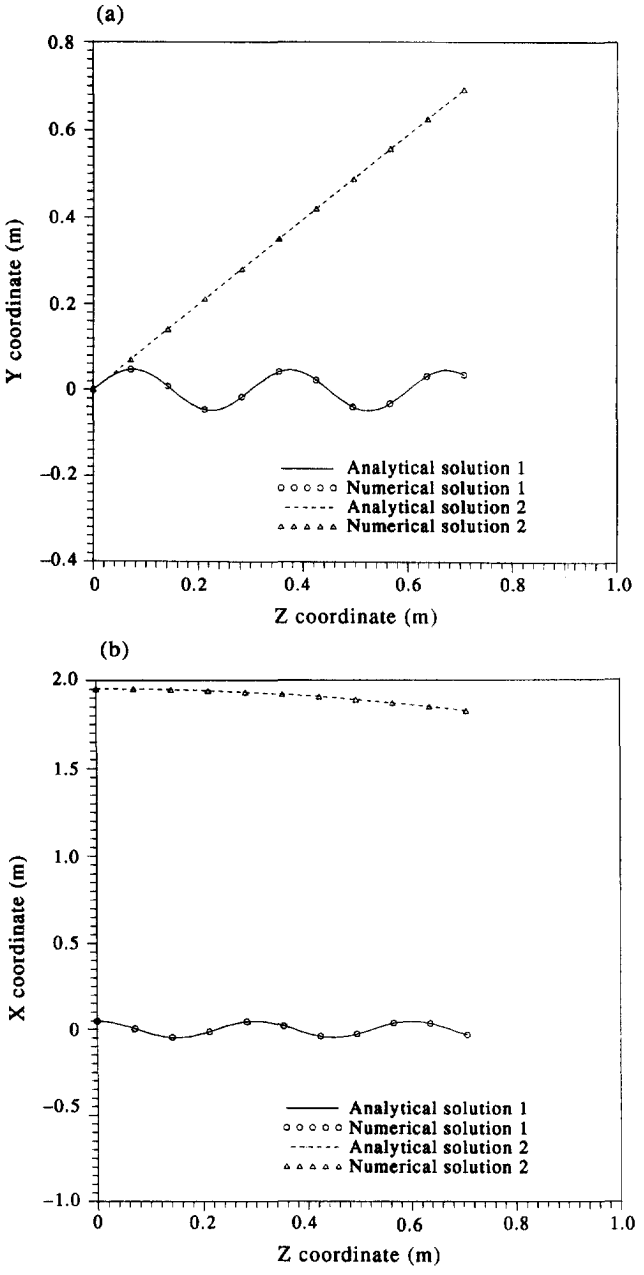

Fig. 3. Geometry of deformed rod, $M_z = 200$ Nm, $F_z = 100$ N, $\alpha = 45°$. (a) ZY plane; (b) ZX plane.

As a further test of the robustness of the numerical solution, the pitch angle of the resulting helix was changed from 45° to first 5° and then 85°, while the values for the axial force and moment were held fixed. This has the effect of changing the relative amounts of bending and twisting in the deformation. When α approaches zero there is almost pure bending with little twist, while a value of α near 90° indicates considerable twist with little bending as the rod remains almost straight. For both these extreme cases considered, eqn (30) still indicates that multiple solutions exist. In all the cases considered, there was again excellent agreement between the analytical and numerical solutions. Also, the checks using κ_1 and the first integral [eqn (3)] were found to be similarly consistent to seven significant digits.

To investigate rods with non-circular cross-sections, the second problem considered is a thin rectangular rod deformed into a Mobius strip. To make such a strip, the ends of the rod are jointed together after undergoing a one-half twist about the centreline. This is an

example of a six-parameter shooting problem as there are six unknown quantities at the start of the rod, specifically the components of the force and moment. The fact that the end of the rod is connected to the start gives three of the six corresponding known values at the end of the rod. The other three conditions arise from the fact that the cross-section at the end of the rod is rotated 180° about the centreline with respect to the orientation of the initial cross-section. The Euler angles needed to specify this orientation supply the remaining known conditions.

Mahadevan and Keller (1993) have recently investigated this problem and presented numerical results for various aspect ratios of the cross-section. An analytical solution available for rods with square cross-sections (aspect ratio = 1) was used as the starting point for a continuation scheme to obtain the results for higher aspect ratios.

Figure 4(a–c) shows the results obtained in the current investigation for a rod (Poisson's ratio = 0) of constant thickness, length of 2π m and which has its width varied to

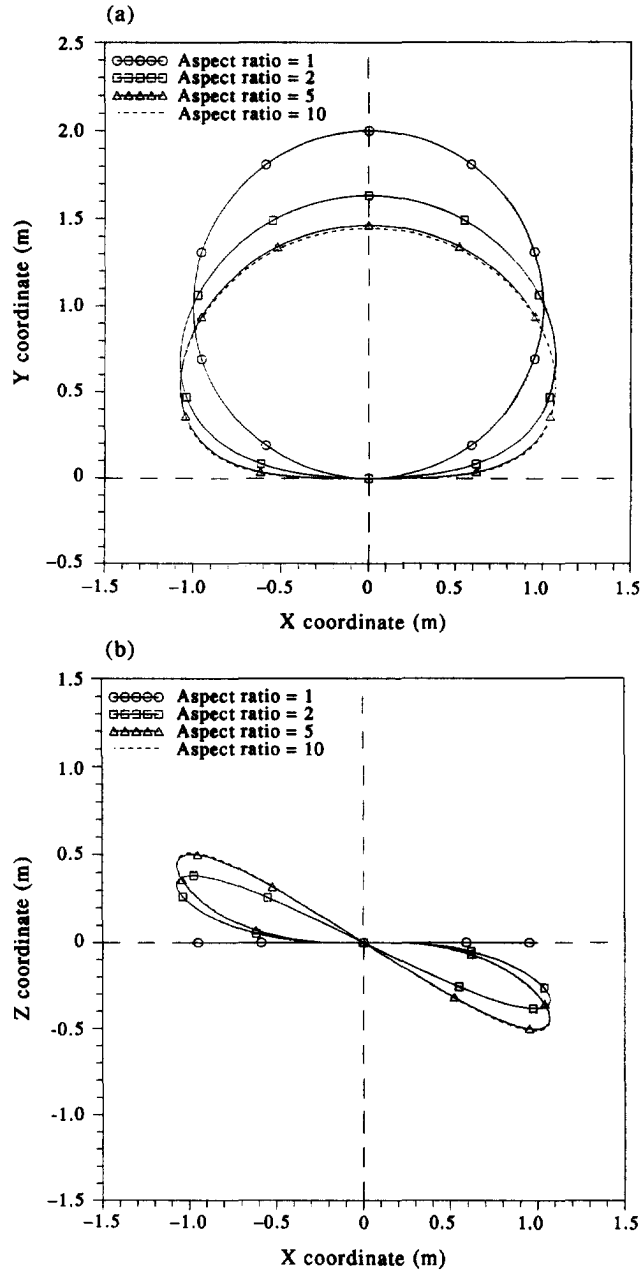

Fig. 4. Geometry of Mobius strip for various aspect ratios. (a) XY plane; (b) XZ plane; (c) YZ plane.

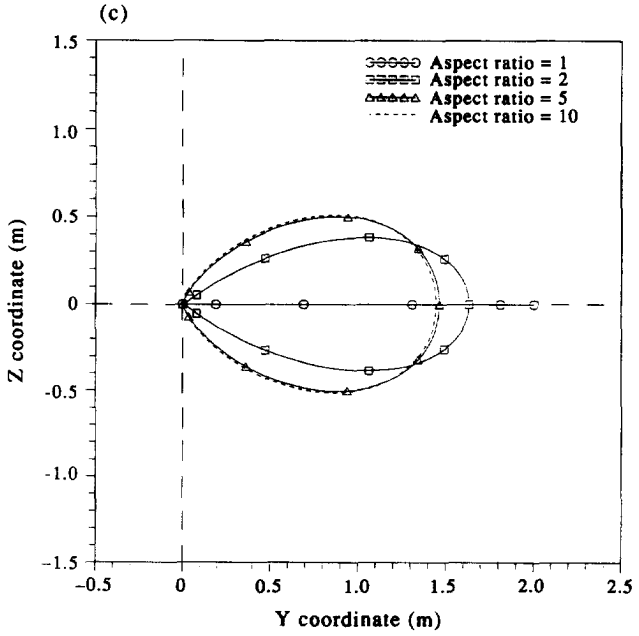

Fig. 4. (*Continued*).

produce aspect ratios in the range from 1 to 10. These results are in close agreement with the graphical results presented by Mahadevan and Keller (1993). For an aspect ratio of 1, the deformed shape of the centreline is circular and remains planar. As the aspect ratio is increased, the centreline deforms more and more out of the initial plane and loses its circular shape [see Fig. 4(b, c)]. For very large aspect ratios, Mahadevan and Keller (1993) showed that the centreline approached a limiting shape, which they found was nearly indistinguishable from the results for an aspect ratio of 10. As a result, higher aspect ratios were not investigated here. For all the cases investigated, the first integral [eqn (3)] was found to show no variation to seven significant digits.

When a square cross-section is used (aspect ratio = 1), the rod is transversely isotropic and, from eqn (6), κ_1 should remain constant. At higher aspect ratios, however, the rod becomes transversely orthotropic and κ_1 need not remain constant. This behaviour is evident in Fig. 5, which shows the variation in κ_1 along the rod for various aspect ratios.

To investigate rods which have an initial curvature, the third problem considered is a cantilever beam with a 45° bend acted upon by a dead tip load, as shown in Fig. 6. This is a two-parameter shooting problem since only the M_1 and M_2 components of the moment are unknown at the fixed end. At the free end all the moment components must vanish.

Table 1 shows the predicted coordinates of the cantilever tip for various dimensionless loads k, where

$$k = \frac{PR^2}{EI} \tag{34}$$

and $EI_2 = EI_3 = EI$. These values are in excellent agreement with the results reported by Surana and Sorem (1989), who used a nonlinear finite element procedure.

The tip load was then replaced with a dead distributed load to consider a more complicated loading and demonstrate the suitability of the current method for handling such loading conditions. Table 2 shows the results obtained for various k_d values, where

$$k_d = \frac{wR^3}{EI} \tag{35}$$

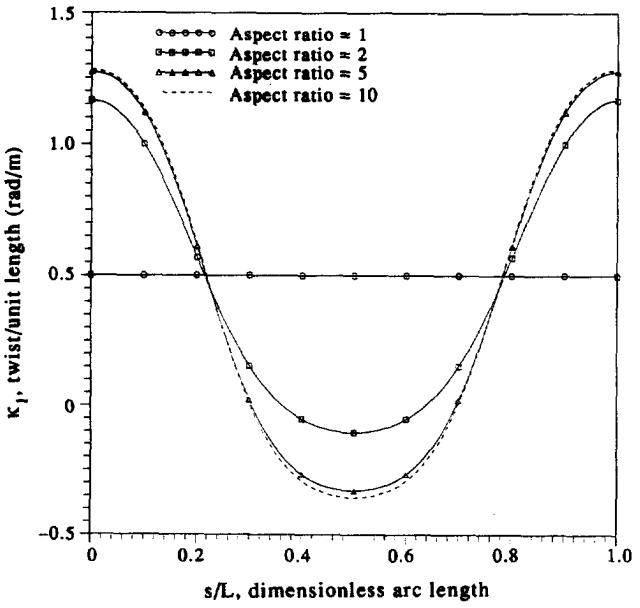

Fig. 5. Twist per unit length along Mobius strip.

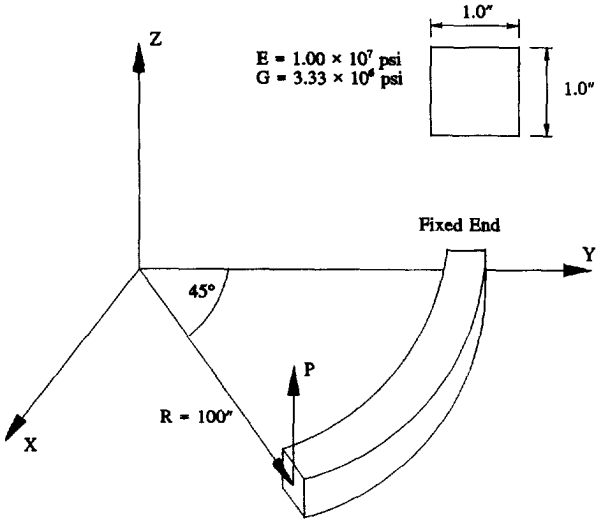

Fig. 6. Initially curved cantilever beam bent out of the plane.

and w is the magnitude of the distributed load. For all of the loads considered, the first integral [eqn (3)] was again found to be consistent to seven significant digits. We were unable to find in the literature another solution which incorporates such a loading condition. Presumably, this implies the difficulty other methods have in solving such problems.

As a final application of the present technique, an orthodontic appliance is considered. Many of these appliances are irregularly formed rods which, when activated, provide a system of forces and couples to reposition teeth within the dental arch. In order to provide appropriate levels of force and moment, these appliances have complex initial geometries and undergo large deflections. The analysis of these structures has been confined to planar deformations (Lipsett *et al.*, 1990); however, in many applications a complete three-dimensional discussion is necessary. An example of a retraction appliance is the T-spring shown in Fig. 7. This spring was constructed of a titanium molybdenum alloy (TMA) wire with a 0.432 mm × 0.625 mm (0.017 in. × 0.025 in.) rectangular cross-section ($E = 73.9$ GPa, $G = 28.2$ GPa). This appliance was analysed for planar deformations by Lipsett *et*

Table 1. Geometry at the end of a curved cantilever due to tip load

	Current method			Surana and Sorem (1989)		
k	X (in.)	Y (in.)	Z (in.)	X (in.)	Y (in.)	Z (in.)
1.0	69.1362	71.6529	15.2722	69.1975	71.6195	15.0119
2.0	65.4006	73.8728	27.5836	65.5727	73.7796	27.2169
3.0	61.0592	76.4225	36.4615	61.3109	76.2900	36.1061
4.0	56.9396	78.8072	42.7314	57.2323	78.6598	42.4276
5.0	53.2915	80.8861	47.2451	53.6011	80.7386	46.9963
6.0	50.1288	82.6567	50.5950	50.4428	82.5185	50.3935
7.0	47.3945	84.1679	53.1595	47.7069	84.0353	52.9962
8.0	45.0206	85.4561	55.1786	45.3285	85.3319	55.0458
9.0	42.9451	86.5639	56.8080	43.2471	86.4472	56.6994
10.0	41.1167	87.5240	58.1511	41.4120	87.4136	58.0621
11.0	39.4935	88.3625	59.2787	39.7818	88.2572	59.2056
12.0	38.0422	89.1002	60.2404	38.3233	88.9990	60.1806
13.0	36.7359	89.7536	61.0719	37.0097	89.6557	61.0232
14.0	35.5530	90.3359	61.7994	35.8195	90.2407	61.7600
15.0	34.4758	90.8580	62.4427	34.7351	90.7649	62.4112

Table 2. Geometry at the end of a curved cantilever due to distributed load

k_d	X (in.)	Y (in.)	Z (in.)
1.0	70.5656	70.7751	4.6391
2.0	70.1384	70.9649	9.1990
3.0	69.4515	71.2698	13.6082
4.0	68.5387	71.6746	17.8090
5.0	67.4398	72.1613	21.7603
6.0	66.1964	72.7111	25.4381
7.0	64.8482	73.3063	28.8330
8.0	63.4307	73.9303	31.9474
9.0	61.9738	74.5716	34.7920
10.0	60.5020	75.2177	37.3826
11.0	59.0343	75.8606	39.7381
12.0	57.5852	76.4940	41.8786
13.0	56.1654	77.1135	43.8238
14.0	54.7824	77.7156	45.5930
15.0	53.4411	78.2985	47.2038

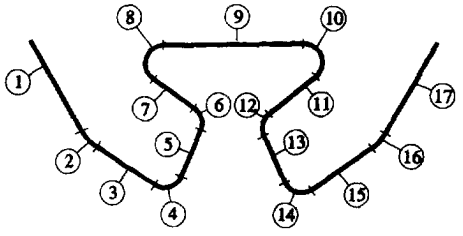

Fig. 7. Initial geometry of orthodontic T-spring appliance.

Table 3. Detailed breakdown of segments used to model orthodontic T-spring

Segment	Length (mm)	Angle (°)	Radius (mm)
1	5.680	—	—
2	—	27.5	2.453
3	3.797	—	—
4	—	100.0	1.000
5	2.765	—	—
6	—	78.0	1.000
7	2.743	—	—
8	—	144.5	−1.000
9	7.725	—	—
10	—	142.0	−1.000
11	3.292	—	—
12	—	76.0	1.000
13	2.765	—	—
14	—	100.0	1.000
15	3.994	—	—
16	—	25.0	2.589
17	5.680	—	—

al. (1990). They used an iterative shooting technique in which the appliance was considered to be composed of the 17 segments shown in Fig. 7. Table 3 shows a detailed breakdown of the segments used to model the appliance. The lengths of the initially straight segments are shown, as are the radii of curvature and arc angles for the initially curved ones. Note that a positive radius is used to specify a counter-clockwise rotation and a negative radius is used for a clockwise rotation.

Figure 8 illustrates the utilization of the T-spring in a plane. The unloaded shape is first brought to the neutral position, essentially through the application of couples to its two ends. The appliance is then further "activated" by pulling the ends apart a specified

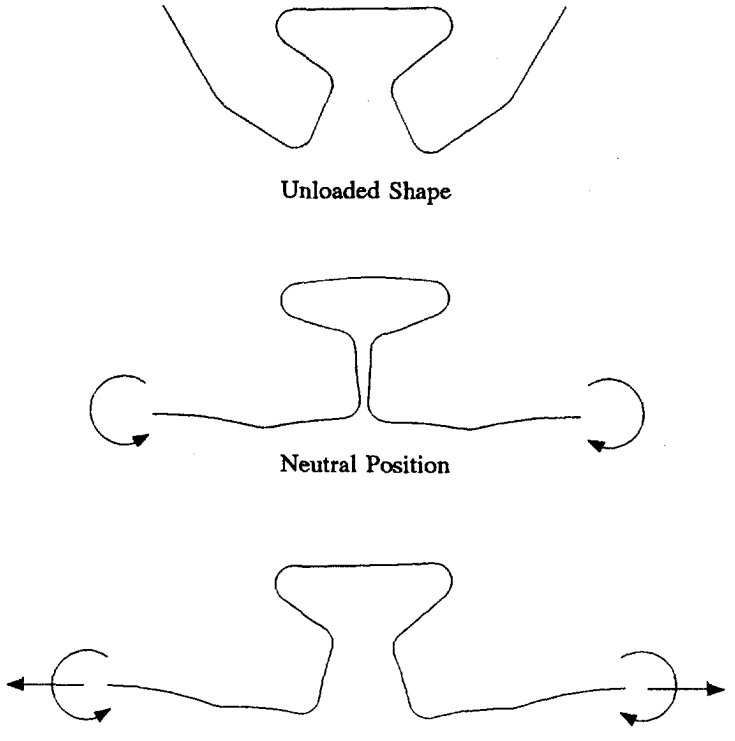

Fig. 8. Undeformed, neutral position and 5 mm activation shape for T-spring appliance.

amount (up to 5 mm in this example). The fully activated spring is then held in this shape by means of brackets which are mounted on the outer surfaces of the teeth. This appliance provides a predictable force/couple system to the teeth on which it is mounted. The T-spring shown is often employed to close up spaces between the teeth (possibly after extraction of a tooth between the two on which the ends are mounted).

While the above description considered only force systems applied in the plane of the appliance, it is often desirable to provide force systems to prevent or enhance out-of-plane movements as well. For example, the application of the planar system of forces alone to the exterior surfaces of the teeth may result in unwanted rotation of the teeth about their long axes. As a possible means of accomplishing this goal, one end of the appliance could then be bent up to 30° out of the initial plane, which would now be a fully three-dimensional deformation. Figure 9(a) and (b) shows two views of the deformed appliance geometry at

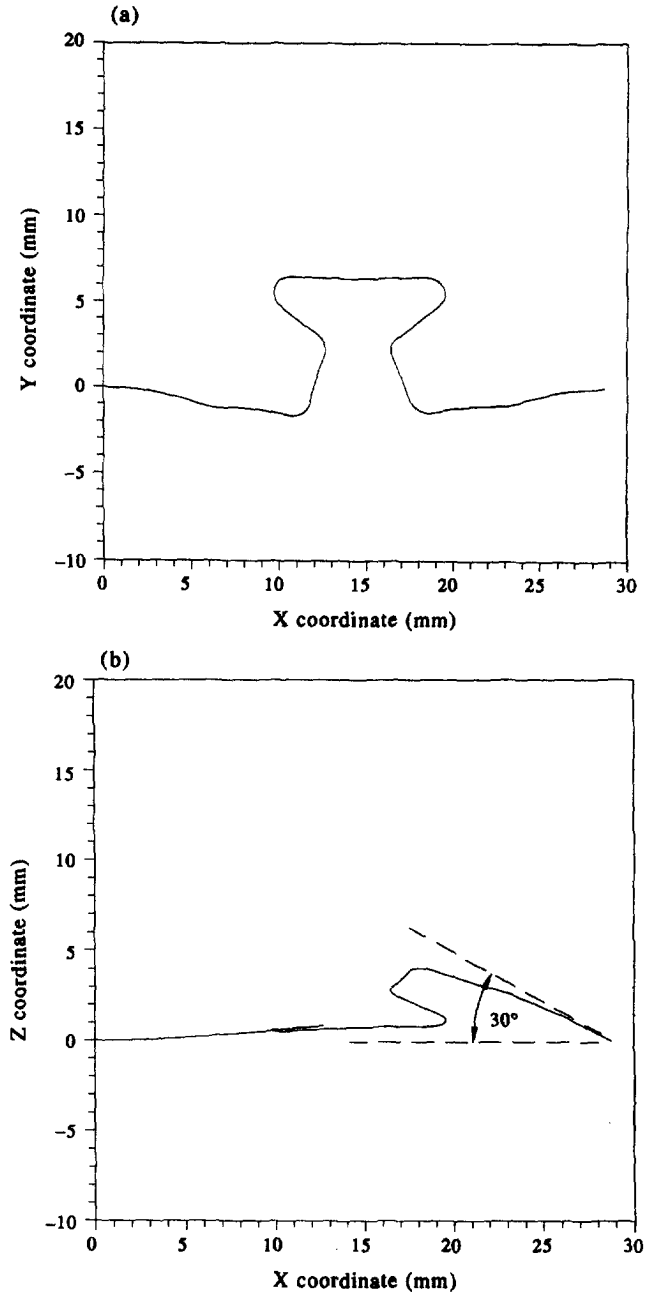

Fig. 9. Deformed geometry of orthodontic appliance; 5 mm activation, 30° out of plane. (a) XY plane; (b) XZ plane.

the maximum activation of 5 mm and the maximum out of plane angulation of 30°. Figure 10(a–f) shows the resulting force and moment components at the left end of the spring. For strictly planar activations (out-of-plane angle = 0), the tension, the vertical shear F_2 and M_3 are the only non-zero components and are essentially identical with the results of Lipsett *et al.* (1990). Figure 10(a), (b) and (f) shows that the out-of-plane deformations imposed on the appliance do not significantly affect these values. They do, however, have a pronounced effect on the other components, namely the horizontal shear F_3 and the additional moment components M_1 and M_2. These components, which are zero for planar activations, show a marked dependence on the out-of-plane angle in Fig. 10(c–e). Results such as these could have significant implications for orthodontic practitioners who are attempting to create specific three-dimensional force systems. Understanding the effects of these out-of-plane deformations may allow the design of better appliances, resulting in fewer unwanted effects and shorter treatment periods.

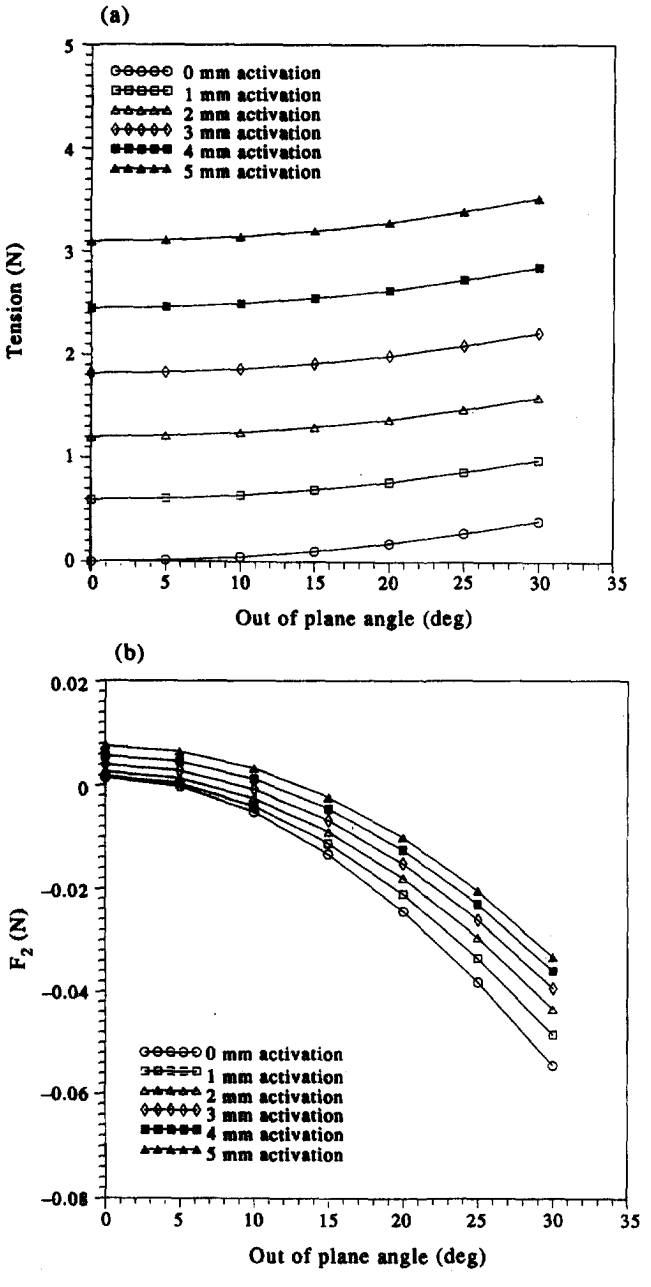

Fig. 10. Force and moment components at left end of appliance. (a) Tension; (b) F_2; (c) F_3; (d) M_1; (e) M_2; (f) M_3.
(*Continued opposite and overleaf.*)

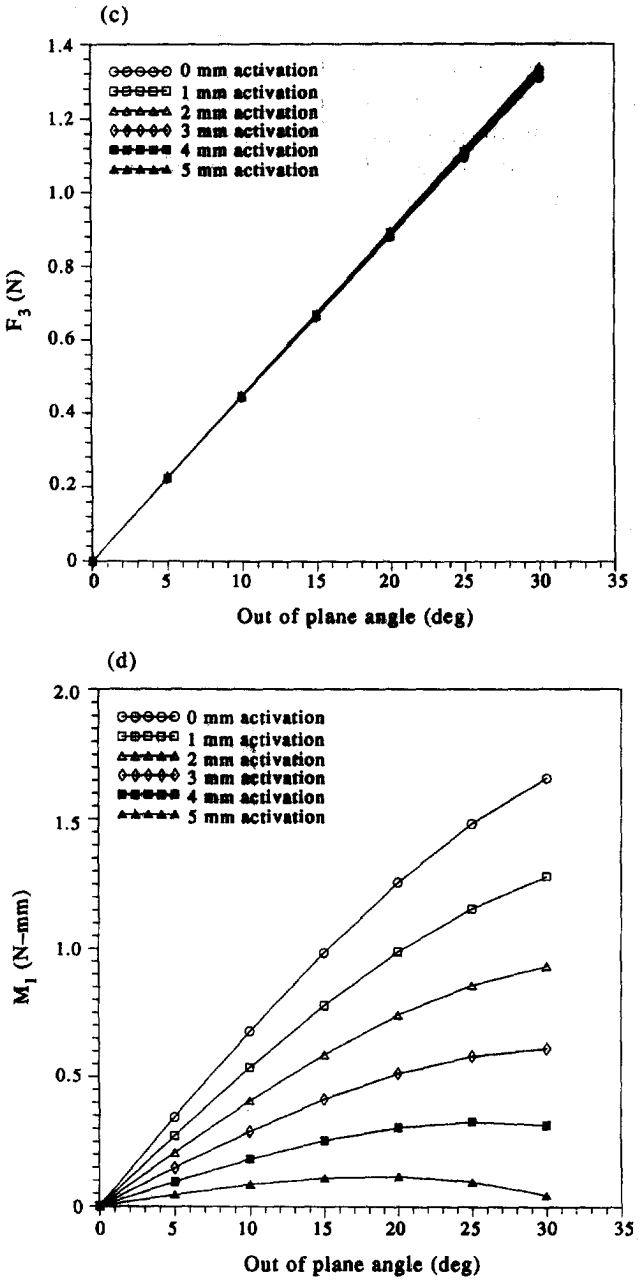

Fig. 10. (*Continued*).

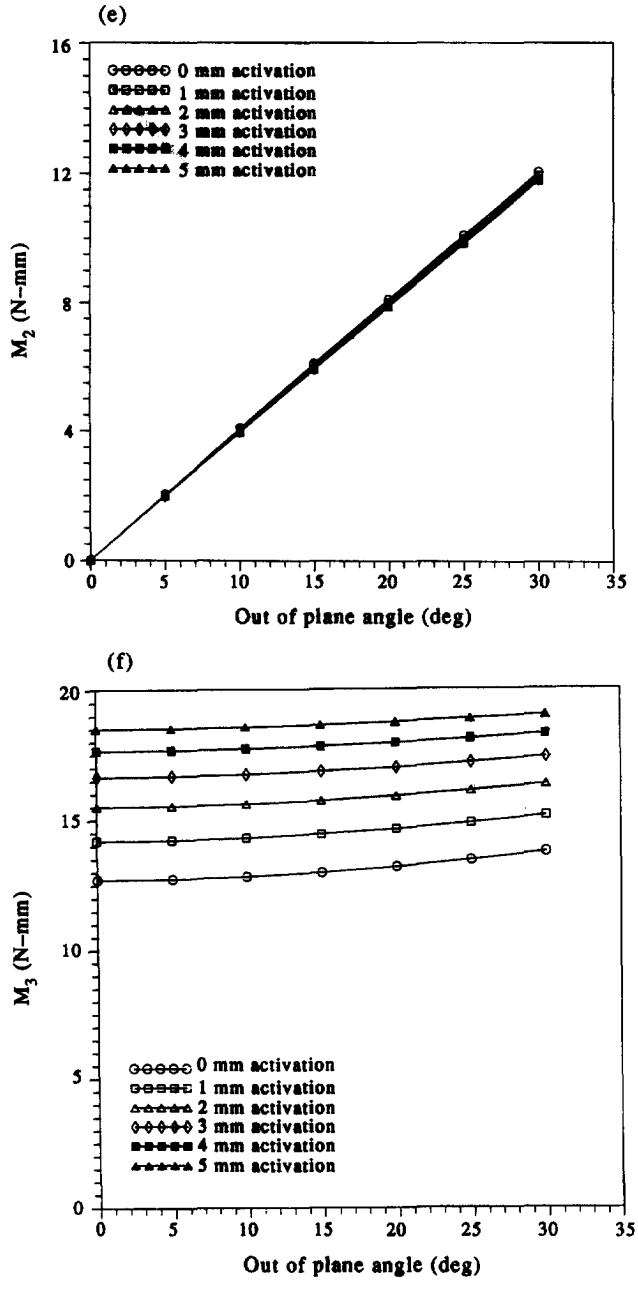

Fig. 10. (*Continued*).

5. CONCLUDING REMARKS

In this paper the two-point boundary value rod problem was solved using an initial value formulation. Converting the original boundary value problem into a sequence of initial value problems in this fashion has its advantages and drawbacks. The most significant difficulty is the fact that good initial estimates of the unknowns are required to ensure that the procedure converges to a solution. This is especially true as the number of unknowns is increased. There are methods available to help alleviate these problems somewhat [so-called globally convergent root finding techniques (Press *et al.*, 1992) or homotopy continuation methods (Keller, 1968)], but good initial estimates are still usually required. In addition, since the equations being considered are highly nonlinear, there is the possibility that multiple solutions may exist for a given problem. The shooting procedure is well suited to finding these solutions, as has been shown previously for planar problems by Faulkner *et al.* (1993) and Lipsett *et al.* (1993).

The solution procedure used also incorporated the division of the rod into segments. There are several advantages to solving the rod in segments in this fashion. The most obvious is that many rods of interest, including orthodontic appliances, have complicated geometries in the undeformed state. Such rods can be thought of as a series of straight, curved, twisted or possibly helical segments. Segmenting the rod in this manner allows a simple, physically intuitive method for modelling such rods. Complex loading conditions or changing material properties can be handled in this manner as well. A further advantage of introducing new segments along the rod is the ability to reset all the Euler angles to 0 and avoid the numerical problems caused by the singularity which occurs at $\theta = \pi/2$.

The procedure as presented is very efficient and is well suited to running on a personal computer. Since each segment is analysed separately, large computer memory is not required as with the finite element procedure. Further, the loads and the large deflections are handled in their entirety in one step, which avoids incremental loading and thus speeds up the calculations significantly. For example, the solutions for the orthodontic appliance at the maximum activation considered converged in nine iterations and required approximately 70 s on a 486 personal computer with a DX2 66 MHz processor. It should be noted that the exact number of iterations required depends on the initial estimates of the unknown conditions. Each iteration required seven passes of the numerical integrator (one to determine the end values and six to compute the partial derivatives required by the false position procedure), since this particular problem is one with six unknowns. Problems with fewer unknowns show better convergence behaviour and require considerably shorter computer time.

In all cases where previous analytical, numerical or experimental results were available, the present method showed excellent agreement. A number of checks on the accuracy of the solutions obtained were also similarly satisfied.

Acknowledgements—The authors wish to acknowledge the support of the Natural Sciences and Engineering Research Council (NSERC) under their scholarship program (D.W.R) and under operating grants OGP 7514 (M.G.F) and OGP 6296 (A.W.L).

REFERENCES

Antman, S. (1968–69). General solutions for plane extensible elasticae having nonlinear stress–strain laws. *Q. J. Appl. Math.* **26,** 35–47.

Defranco, J. C., Koenig, H. A. and Burstone, C. J. (1976). Three dimensional large displacement analysis of orthodontic appliances. *J. Biomech.* **9,** 793–801.

Faulkner, M. G., Lipsett, A. W., El-Rayes, K. and Haberstock, D. L. (1991). On the use of vertical loops in retraction systems. *Am. J. Orthodont. Dentofac. Orthop.* **99,** 328–336.

Faulkner, M. G., Lipsett, A. W. and Tam, V. (1993). On the use of a segmental shooting technique for multiple solutions of planar elastica problems. *Comput. Meth. Appl. Mech. Engng* **110,** 221–236.

Faulkner, M. G. and Stredulinsky, D. C. (1976–77). Nonlinear bending of inextensible thin rods under distributed and concentrated loads. *Trans. CSME* **4,** 77–81.

Fried, I. (1981). Stability and equilibrium of the straight and curved elastica—finite element computation. *Comput. Meth. Appl. Mech. Engng* **28,** 49–61.

Frisch-Fay, R. (1962). *Flexible Bars*. Butterworths, London.

Goldstein, H. (1980). *Classical Mechanics*, 2nd edn. Addison-Wesley, Reading, MA.

Keller, H. B. (1968). *Numerical Methods for Two-Point Boundary Value Problems*. Blaisdell, Waltham, MA.

Landau, L. D. and Lifshitz, E. M. (1986). *Theory of Elasticity*, 3rd edn. Pergamon Press, Oxford.
Lipsett, A. W., Faulkner, M. G. and El-Rayes, K. (1990). Large deformation analysis of orthodontic appliances. *ASME J. Biomech. Engng* **112**, 29–37.
Lipsett, A. W., Faulkner, M. G. and Tam, V. (1993). Multiple solutions for inextensible arches. *Trans. CSME* **17**, 1–15.
Love, A. E. H. (1944). *A Treatise on the Mathematical Theory of Elasticity*. Dover, New York.
Mahadevan, L. and Keller, J. B. (1993). The shape of a Möbius band. *Proc. R. Soc. Lond.* **440**, 149–162.
Mitchell, T. P. (1959). The nonlinear bending of thin rods. *ASME J. Appl. Mech.* **26**, 40–43.
Navaee, S. and Elling, R. E. (1991). Large deflections of cantilever beams. *Trans. CSME* **15**, 91–107.
Navaee, S. and Elling, R. E. (1992). Equilibrium configurations of cantilever beams subjected to inclined end loads. *ASME J. Appl Mech.* **59**, 572–579.
Press, W. H., Teukolsky, S. A., Vetterling, W. T. and Flannery, B. P. (1992). *Numerical Recipes*, 2nd edn. Cambridge University Press, Cambridge.
Steigmann, D. J. and Faulkner, M. G. (1993). Variational theory for spatial rods. *J. Elast.* **33**, 1–26.
Surana, K. S. and Sorem, R. M. (1989). Geometrically nonlinear formulation for three dimensional curved beam elements with large rotations. *Int. J. Numer. Meth. Engng* **28**, 43–73.
Wang, C. Y. (1986). A critical review of the heavy elastica. *Int. J. Mech. Sci.* **28**, 549–559.
Whitman, A. B. and DeSilva, C. N. (1974). An exact solution in the nonlinear theory of rods. *J. Elast.* **4**, 265–280.